Available online at www.sciencedirect.com
ScienceDirect
International Journal of Heat and Fluid Flow 28 (2007) 1027–1033
International Journal of HEAT AND FLUID FLOW
www.elsevier.com/locate/ijhff

Numerical study of slip flow heat transfer of non-Newtonian fluids in circular microchannels

M. Barkhordari, S.Gh. Etemad *

Chemical Engineering Department, Isfahan University of Technology, Isfahan 84156, Iran

Received 17 August 2005; received in revised form 5 February 2007; accepted 20 February 2007
Available online 11 April 2007

Abstract

In the present investigation, numerical simulations are performed to study flow and thermal fields of non-Newtonian fluids in circular microchannels. The flow is considered to be slip, axisymmetric, steady, incompressible, laminar, and power law model is used to characterize the behavior of the non-Newtonian fluid. The constant wall heat flux and constant wall temperature are employed as thermal boundary conditions. The set of governing dimensionless differential equations with appropriate boundary conditions are solved together using control volume finite difference method. Results indicate the increasing slip coefficient decreases the product of friction factor and Reynolds number and centerline velocity while results in increasing of local Nusselt numbers. Slip effect enhances with increasing power law index. Also slip effect in constant wall heat flux is more than that of constant wall temperature boundary conditions.

Keywords: Forced convection; Non-Newtonian; Power law; Microchannel; Slip velocity; Numerical simulation

1. Introduction

Microchannels are used in several industries and equipments such as cooling of electronic package, microchannel heat sinks (Mudawar and Qu, 2002), microchannel heat exchangers, microchannel fabrication (Simoes et al., 1998), cooling and heating of different devices (Adams, 1998; Zengerle and Richter, 1994). As the size of a channel is reduced, the continuum flow assumption is no longer valid; however there is a certain value for the size that one can still apply Navier–Stokes equations with some modifications on the boundary conditions (Arkailic et al., 1994; Shih et al., 1996). The flow in these conditions is called slip flow. Generally, hydrodynamic wall boundary conditions are sorted as below:

(1) No-slip boundary condition.
(2) Slip boundary condition.

Continuous hydrodynamics describes fluids flow in wide range of systems and sizes but in some systems no-slip boundary condition is not valid. For example in polymeric fluids flow and gas flow in nano and micro pores and channels and in Micro Electro Mechanical systems (MEMS), slip occurs near the wall and the wall velocity is non-zero. Knudsen number (Kn) is defined to represent the rarefaction effects and amount of continuous behavior of gases. It is the ratio of the mean free path to the characteristic length of the channel. By increasing Kn first continuum flow changes into slip flow and then transition regime and finally regime of gas will be free molecule.

Beskok and Karniadakis (1994) give the range for the Knudsen number in slip-flow regime as $0.001 < Kn < 0.1$. Koplik and Banavar (1995), Golden (1964) and Paranjape and Robson (1990) found that in some cases there is not conformity in wall friction considering zero velocity on wall and claimed that it is possible wall velocity be non-zero.

Maxwell (1878) and Eirich (1978) proposed a relation for slip velocity of gases that slip velocity was defined as function of fluid molecular properties, surface and wall shear

* Corresponding author. Tel.: +98 311 3915625; fax: +98 311 3912677.
E-mail address: etemad@cc.iut.ac.ir (S.Gh. Etemad).

0142-727X/$ - see front matter © 2007 Elsevier Inc. All rights reserved.
doi:10.1016/j.ijheatfluidflow.2007.02.007

Nomenclature

A	defined by Eq. (6), dimensionless
B	defined by Eq. (7), dimensionless
C	defined by Eq. (8), dimensionless
C_p	heat capacity, J/kg K
D	defined by Eq. (9), dimensionless
D_h	hydraulic diameter, m
E	defined by Eq. (10), dimensionless
F	defined by Eq. (11), dimensionless
f	friction factor $\left[=\frac{\tau_w}{1/2\rho u_e^2}\right]$, dimensionless
H	constant wall heat flux boundary condition
K	thermal conductivity, W/m K
K_0	consistency index at reference temperature, N s^n/m^2
n	power law index, dimensionless
Nu	local Nusselt number $\left[=\frac{1}{\theta_w-\theta_b}$ for H and $\frac{\partial\theta}{\partial R}\frac{}{\theta_b}$ for T boundary conditions], dimensionless
p	pressure, Pa
P	dimensionless pressure $\left[=\frac{p-p_0}{\rho u_e^2}\right]$
P_0	pressure at the inlet, Pa
Pe	Peclet number [$=Pr\,Re$], dimensionless
Pr	Prandtl number $\left[=\frac{K_0 C_p\left(\frac{u_e}{D_h}\right)^{n-1}}{K}\right]$, dimensionless
q	heat flux, W/m^2
r	radial coordinate, m
R	dimensionless radial coordinate $\left[=\frac{r}{D_h}\right]$, dimensionless
Re	Reynolds number $\left[=\frac{\rho U_e^{2-n} D_h^n}{K_0}\right]$, dimensionless
T	temperature, constant wall temperature boundary condition, °C
u	axial velocity, m/s
U	dimensionless axial velocity $\left[=\frac{u}{u_e}\right]$, dimensionless
v	radial velocity, m/s
V	dimensionless radial velocity $\left[=\frac{v}{u_e}\right]$, dimensionless
x	axial distance, m
X	dimensionless axial distance $\left[=\frac{x}{D_h}\right]$, dimensionless
X^+	dimensionless axial coordinate $\left[=\frac{x}{D_h\cdot Re}\right]$, dimensionless
X^*	dimensionless axial coordinate $\left[=\frac{x}{D_h\cdot Re\cdot Pr}\right]$, dimensionless

Greek symbols

β_s	slip coefficient $\left[=\frac{u_s}{u_m}\right]$, dimensionless
Δ	deformation tensor in cylindrical coordinate, s^{-1}
θ	dimensionless temperature $\left[=\frac{T-T_e}{qD_h/K}$ for H and $\frac{T-T_w}{T_e-T_w}$ for T boundary conditions]
θ_b	dimensionless bulk temperature $\left[=\frac{\int U\theta\,dA}{\int U\,dA}\right]$
ρ	density, kg/m^3
τ	shear stress, N/m^2

Subscripts

c	centerline value
e	evaluated at entrance condition
H	evaluated for H boundary condition
m	mean value
s	slip value
T	evaluated for T boundary condition
w	evaluated at wall condition

stress. The more complete model was offered by Eirich (1978) in which the slip velocity was a function of wall shear stress. Since the boundary condition for the fluid flow through the channels plays a key role on the hydrodynamic behavior, extensive investigations were done and based on the results several researchers have suggested that the well-accepted no-slip boundary condition may not be suitable for flows at the micro and nano scale (Watanabe et al., 1998, 1999; Ruckenstein and Rajora, 1983; Pit et al., 2000; Zhu and Granick, 2001; Tretheway and Meinhart, 2002). Although no-slip boundary condition is a practical condition for fluid mechanics but happening of slip near the wall has created a challenging problem for fluid mechanics and non-Newtonian fluids and slip of fluid in polymeric melts and solutions has been importance of several investigations (Wang, 1999; Léger et al., 1999). Many mechanisms have been proposed to explain this phenomenon but those that have received wider acceptance in recent years are polymer chain disentanglement (Brochard and de Gennes, 1992) and debonding (Hill, 1998) at the wall–polymer interface. Many models were developed earlier, which proposed that slip occurs by constitutive (bulk) instability (Malkus et al., 1990; Mcleish and Ball, 1986; Lin, 1985). However, it has now been shown unambiguously that slip is an interfacial phenomenon that occurs very close to the wall. Although the mechanisms for wall-slip are fairly well understood, there are several issues that still remain unresolved. For example, the dynamics of polymer chains at the wall is not yet well understood, and so is the effect of molecular parameters such as molecular weight distribution and long and short chain branching (Yang et al., 1998).

The physical manifestation of slip shows up in terms of experimental observations of the existence of a critical wall-shear stress, flow oscillations, extrudate distortion, hysteresis and temperature dependence of critical wall-shear stress. However, by merely observing a given mani-

festation in a given set of experimental data, it has not been possible so far to a priori assign a mechanism, be it debonding or disentanglement. Indeed the same experimental data on slip for the same polymer have been interpreted in terms of both disentanglement as well as debonding. For example, the experimental data on wall slip for common systems such as polyethylene in steel capillaries has been described by theoretical arguments of debonding as well as disentanglement. Slip occurs when any one of the types of junctions is destroyed. If the junctions at the wall are destroyed, then the slip occurs by debonding. When the entanglement junctions are destroyed, the slip occurs by disentanglement (Yogesh et al., 2000).

Tunc and Bayazitoglu (2000) have investigated slip effect in rectangular microchannels and they defined slip velocity as a constant coefficient of mean velocity of fluid (Tunc and Bayazitoglu, 2002).

Velocity slip and temperature jump are the two major effects of reducing the size of channel cross section. Convection heat transfer in circular and non-circular microchannels has been solved over the years (Harms et al., 1999; Qu et al., 2000; Sparrow and Lin, 1962; Ameel et al., 1997; Tunc and Bayazitoglu, 2000; Tunc and Bayazitoglu, 2001). In these studies, the effects of velocity slip and temperature jump at the wall and viscous dissipation were considered. The main finding was that velocity slip and temperature jump have opposite effects on heat transfer. Although the velocity slip tends to increase the Nusselt number, the temperature jump tends to decrease it. The inclusion the viscous heating increases the Nusselt number for the fluid being cooled and decreases it for the fluid being heated.

Owhaib and Palm (2004) investigated experimentally about the heat transfer characteristics of single-phase forced convection through single circular microchannels with 1.7, 1.2, and 0.8 mm as inner diameters. The results were compared both to correlations for the heat transfer in macroscale channels and to correlations suggested for microscale geometries. The results show good agreement between the classical correlations and the experimentally measured data in the turbulent region. Contrary, none of the suggested correlations for microchannels, agreed with the test data. Morini (2004) has collected a review of experimental results about single phase convective heat transfer in microchannels in the wide range of hydraulic diameter and different fluids. Celeta (2004) collected useful information about the fluid flow and heat transfer through microchannels.

Generally, there is a lack of information in the literature regarding the flow and heat transfer of non-Newtonian fluids through microchannels. Therefore, in this study the forced convection heat transfer of power law model non-Newtonian fluids through circular microchannels at entrance region as well as developed section were considered and to present the velocity slip, a parameter called slip coefficient was defined as the ratio of the velocity of the fluid at the wall to the mean velocity.

2. Modelling and analysis

This numerical study is concerned with simultaneous development of flow and heat transfer for power law fluids. The constant wall temperature (T) and constant wall heat flux (H) are considered as thermal boundary conditions. It covers the effect of slip coefficients for different power law indices.

The problem to be considered is depicted schematically in Fig. 1. The symmetry of the computational domain permits the restriction of solution to only half the circular microchannel. All fluid properties are held constant. The Ostwald–de Waele power law is used to model shear stress in following form (Bird et al., 1987):

$$\tau = K_0 \mathrm{e}^{\frac{T_0}{T}} \left| \frac{1}{2} \Delta : \Delta \right|^{\frac{n-1}{2}} \Delta \tag{1}$$

where K_0 is the consistency index at reference temperature (T_0) and n is the power law index.

The dimensionless governing equations in cylindrical coordinate can be written as:

Continuity:

$$\frac{1}{R}\frac{\partial (RV)}{\partial R} + \frac{\partial U}{\partial X} = 0 \tag{2}$$

R-momentum:

$$V\frac{\partial V}{\partial R} + U\frac{\partial V}{\partial X} = -\frac{\partial P}{\partial R} + \frac{1}{Re}\left(\frac{1}{R}\frac{\partial A}{\partial R} - B + \frac{\partial C}{\partial X}\right) \tag{3}$$

X-momentum:

$$V\frac{\partial U}{\partial R} + U\frac{\partial U}{\partial X} = -\frac{\partial P}{\partial X} + \frac{1}{Re}\left(\frac{1}{R}\frac{\partial D}{\partial R} + \frac{\partial E}{\partial X}\right) \tag{4}$$

Energy:

$$V\frac{\partial \theta}{\partial R} + U\frac{\partial \theta}{\partial X} = \frac{1}{Pe}\left[\frac{1}{R}\frac{\partial}{\partial R}\left(R\frac{\partial \theta}{\partial R}\right) + \frac{\partial^2 \theta}{\partial X^2}\right] \tag{5}$$

where

$$A = 2Re^{\frac{T_0}{T}} F \frac{\partial V}{\partial R} \tag{6}$$

$$B = 2\mathrm{e}^{\frac{T_0}{T}} F \frac{V}{R^2} \tag{7}$$

$$C = \mathrm{e}^{\frac{T_0}{T}} F \left(\frac{\partial U}{\partial R} + \frac{\partial V}{\partial X}\right) \tag{8}$$

$$D = Re^{\frac{T_0}{T}} F \left(\frac{\partial U}{\partial R} + \frac{\partial V}{\partial X}\right) \tag{9}$$

$$E = 2\mathrm{e}^{\frac{T_0}{T}} F \frac{\partial U}{\partial X} \tag{10}$$

$$F = \left\{ 2\left[\left(\frac{\partial V}{\partial R}\right)^2 + \left(\frac{V}{R}\right)^2 + \left(\frac{\partial U}{\partial X}\right)^2\right] + \left(\frac{\partial U}{\partial R} + \frac{\partial V}{\partial X}\right)^2 \right\}^{\frac{n-1}{2}} \tag{11}$$

The fluid enters the circular microchannels with uniform velocity and temperature profiles. Thus:

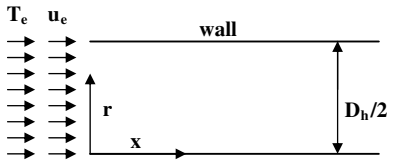

Fig. 1. Computational domain of circular microchannel.

$$X=0\begin{cases} U=1, \quad V=0 \\ \theta=1 \quad \text{for } T \text{ boundary condition} \\ \theta=0 \quad \text{for } H \text{ boundary condition} \end{cases} \tag{12}$$

The slip condition is applied at the microchannel walls and the dimensionless axial velocity at walls is β_s (Tunc and Bayazitoglu, 2002) which is defined as $\frac{u_s}{u_m}$.

The dimensionless temperature at the walls for the T boundary condition is zero and for H boundary condition the dimensionless heat flux at wall is unity. The velocity and temperature gradient across the symmetry axis is zero. Thus:

$$\begin{cases} \dfrac{\partial U}{\partial R}=\dfrac{\partial V}{\partial R}=0 \\ \dfrac{\partial \theta}{\partial R}=0 \end{cases} \tag{13}$$

A fully developed condition could be prescribed at outlet boundary.

In the present study Eqs. (2)–(11), which are an elliptic systems of partial differential equations with associated boundary conditions, were solved using control volume finite difference method. The control volume finite difference method is well documented in the literature by Patankar (Patankar, 1980).

3. Results and discussion

The flow and heat transfer domain was discretized and the governing equations (continuity, momentum and energy), were converted into algebraic equations using 20×3000 grids. The number of meshes was based on the requirement of mesh independence of the solution. Due to the higher velocity and temperature gradients in the entrance region and in the vicinity of the wall, finer mesh distributions were used in these regions.

The accuracy of numerical procedure was tested by comparing the results of some specific cases with available analytical and numerical solutions. Tables 1 and 2 show the excellent agreement between the no-slip fully developed friction factor and local Nusselt number for H and T boundary conditions for different power law indices of the present investigation and analytical solutions available in the literature (Eqs. (14)–(16), Etemad, 1995; Datta, 1999; Bird et al., 2002)

Table 1
Comparison of the developed U_{max} and $f\cdot Re$ obtained from present study and Eqs. (14), (15) for no-slip condition

n	0.50	1.00	1.25
U_{max} (Eq. (14))	1.67	2.00	2.11
U_{max} (present study)	1.66	1.99	2.11
$f\cdot Re$ (Eq. (15))	6.32	16.00	25.24
$f\cdot Re$ (present study)	6.30	15.90	25.04

Table 2
Comparison of fully developed local Nusselt number for no-slip condition

n	0.50	1.00	1.25
Nu_T	3.949 (Bird et al., 2002) 3.950 (Etemad, 1995)	3.659 (Bird et al., 2002) 3.657 (Etemad, 1995)	3.590 (Etemad, 1995)
Nu_T (present study)	3.920	3.620	3.550
Nu_H (Eq. (16))	4.740	4.360	4.280
Nu_H (present study)	4.740	4.350	4.260

$$U_{max}=\frac{3n+1}{n+1} \tag{14}$$

$$f\cdot Re=2^{n+1}\left(\frac{3n+1}{n}\right)^n \tag{15}$$

$$Nu_H=\frac{n+1}{3n+1}\Big/\left\{\left[\frac{1}{4}-\frac{n^2}{(3n+1)^2}\right]-\frac{3n+1}{5n+1}\left[\frac{1}{8}-\frac{n^3}{(3n+1)^3}\right]\right\} \tag{16}$$

The dimensionless centerline axial velocity and friction factor are presented in Figs. 2 and 3 for different values of slip coefficients, while the data for fully developed maximum axial velocities and friction factors are tabulated at Tables 3 and 4, respectively. From Fig. 2, the centerline and maximum axial velocity for different slip coefficients increase with increasing of axial distance which is related to flow development. Also from Fig. 2 and Table 3 the maximum velocity decreases with increasing the slip coefficient. When slip flow occurs, axial velocity of fluid near wall increases and requirement of mass conservation forces the fluids to correspondingly slow down in the center of

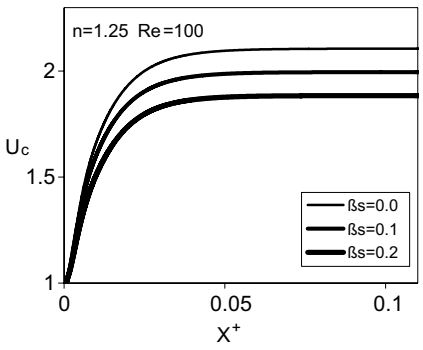

Fig. 2. The effect of slip coefficient on centerline velocities.

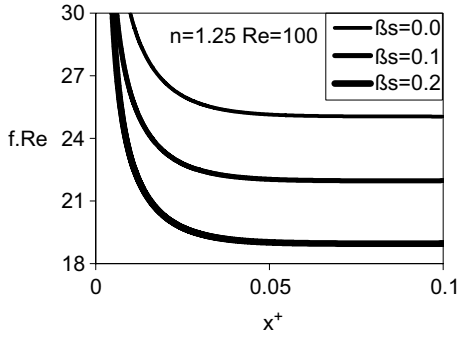

Fig. 3. The effect of slip coefficient on friction factors.

Table 3
Comparison of the developed U_{max} for different slip coefficients

β_s	0.2	0.1
$U_{max}\|_{n=0.5}$	1.53	1.59
$U_{max}\|_{n=1}$	1.79	1.89
$U_{max}\|_{n=1.25}$	1.88	2.00

Table 4
Comparison of developed $f \cdot Re$ for different slip coefficients

n	1.25	1.00	0.50
$f \cdot Re\|_{\beta_s=0.0}$	25.04	15.90	6.30
$f \cdot Re\|_{\beta_s=0.1}$	21.95	14.31	5.97
$f \cdot Re\|_{\beta_s=0.2}$	18.95	12.72	5.63
Relative difference percent: $\frac{f\cdot Re\|_{\beta_s=0.0}-f\cdot Re\|_{\beta_s=0.2}}{f\cdot Re\|_{\beta_s=0.0}}\times 100$	24.32	20.00	10.63

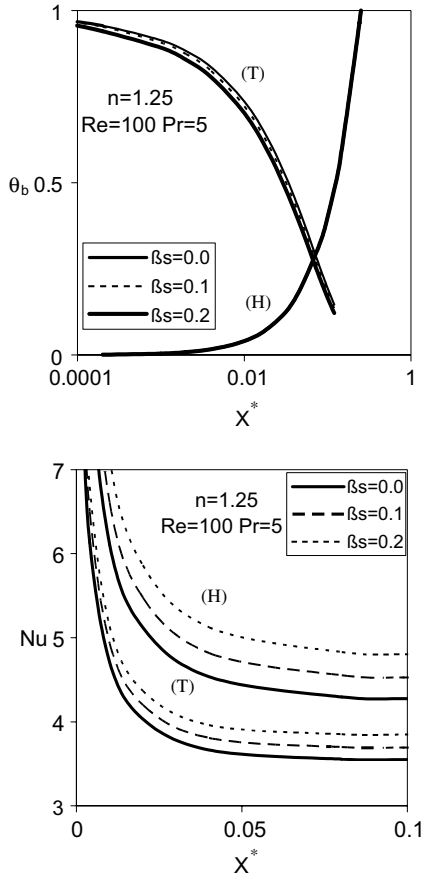

Fig. 4. The effect of slip coefficient on dimensionless bulk temperatures and local Nusselt numbers for H and T boundary conditions.

microchannel (Table 3). From Fig. 3, the friction factor decreases with increasing of axial distance which relates to the high pressure drop in the developing section of the channel. The slip flow results in smaller wall shear stress, consequently friction factor decreases. Also, power law index has strong effect on the performance of slip velocity. From Table 4, the effect of slip coefficient becomes important with increasing power law index. Consequently slip effects for dilatant fluids are stronger than that of pseudo-plastic fluids.

The local and also fully developed Nusselt numbers and dimensionless bulk temperatures for different power law indices and for various slip coefficients and boundary conditions are presented through Fig. 4 and Table 5. From Fig. 4 and Table 5, local Nusselt numbers increase with increasing the slip coefficients. When slip flow occurs, axial velocity of fluid near wall increases which promotes the role of convection heat transfer and results in higher Nusselt number. Also based on the results of Table 5, slip effects in dilatant fluids are stronger than that of pseudo-plastic fluids. For H boundary condition, the wall temperature gradient is more than that of T boundary conditions. Consequently the slip effect in constant wall heat flux case is more than that of constant wall temperature boundary condition (Table 5).

Table 5
Comparison of fully developed local Nusselt numbers for different power law indices and slip coefficients for H and T boundary conditions

n	0.50	1.00	1.25
$Nu_H\|_{\beta_s=0.0}$	4.74	4.35	4.26
$Nu_H\|_{\beta_s=0.1}$	4.97	4.60	4.51
$Nu_H\|_{\beta_s=0.2}$	5.22	4.87	4.79
$Nu_T\|_{\beta_s=0.0}$	3.92	3.62	3.55
$Nu_T\|_{\beta_s=0.1}$	4.04	3.76	3.69
$Nu_T\|_{\beta_s=0.2}$	4.18	3.84	3.91
Relative difference percent (H): $\frac{Nu_H\|_{\beta_s=0.2}-Nu_H\|_{\beta_s=0.0}}{Nu_H\|_{\beta_s=0.0}}\times 100$	10.13	11.95	12.44
Relative difference percent (T): $\frac{Nu_T\|_{\beta_s=0.2}-Nu_T\|_{\beta_s=0.0}}{Nu_T\|_{\beta_s=0.0}}\times 100$	6.63	8.01	8.17

The local Nusselt numbers and dimensionless bulk temperatures for different Prandtl numbers and for various slip boundary conditions are presented in Fig. 5. From this figure, for slip conditions the local Nusselt number increases with increasing of Prandtl number. Also from Fig. 6, increasing Reynolds number enhances the local Nusselt number for both thermal boundary conditions. From the results increasing Reynolds number, Prandtl number and slip coefficient has significant effects on dimen-

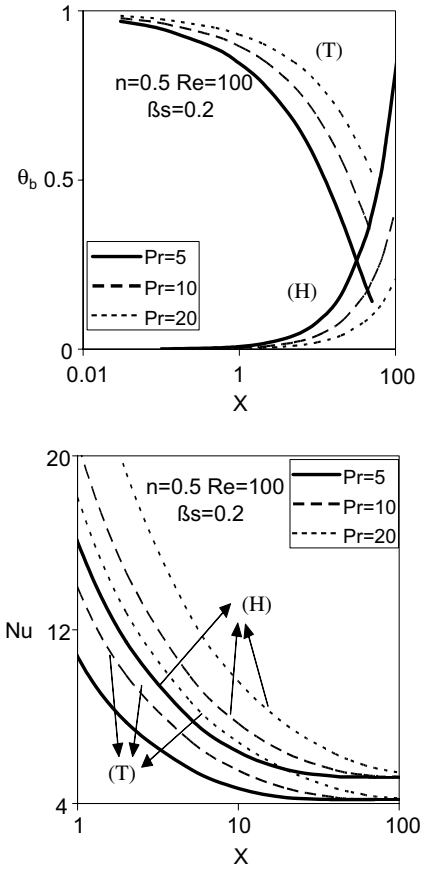

Fig. 5. The effect of Prandtl number on dimensionless bulk temperatures and local Nusselt numbers for H and T boundary conditions.

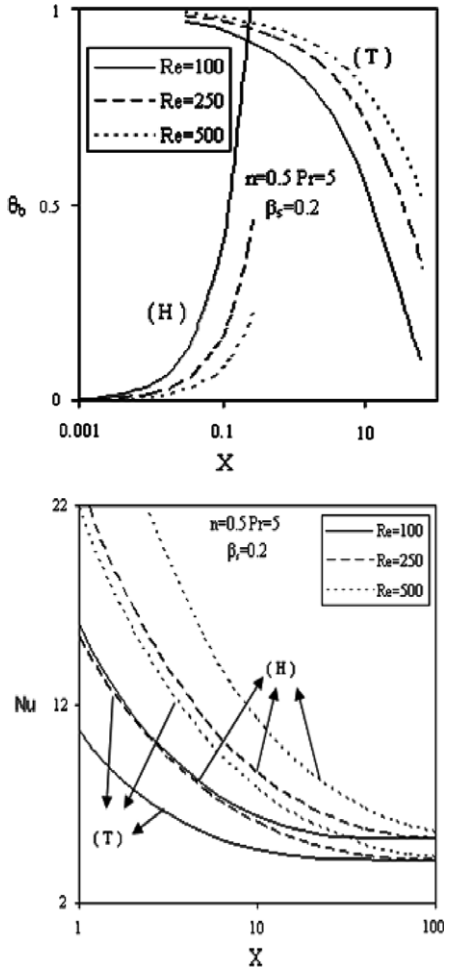

Fig. 6. The effect of Reynolds number on dimensionless bulk temperatures and local Nusselt numbers for H and T boundary conditions.

sionless bulk temperature for both thermal boundary conditions.

4. Conclusions

In the present investigation, numerical study is carried out to investigate about flow and thermal field of non-Newtonian fluids flowing through circular microchannels. Results show the product of friction factor and Reynolds number and centerline velocity increase with increasing power law index while considering wall slip condition results in reduction of those parameters. Relative difference of the product of friction factor and Reynolds number between slip and no-slip conditions is enhanced with increasing power law index. Consequently slip effects for dilatant fluids are stronger than that of pseudoplastic fluids. Increasing slip coefficient enhances the local Nusselt number for both thermal boundary conditions. Also relative difference of the Nusselt number between slip and no-slip conditions increases for higher power law indices. Results indicate the effect of slip condition is more important for H boundary condition. When slip effect occurs, increasing Reynolds number and Prandtl number enhances the local Nusselt number and has significant effect on dimensionless bulk temperature for both thermal boundary conditions.

References

Adams, T.M., 1998. Turbulent convection in microchannels. Ph.D. thesis, Georgia Institute of Technology, Atlanta, GA.

Ameel, T.A., Barron, R.F., Wang, X., Warrington, R.O., 1997. Laminar forced convection in a circular tube with constant heat flux and slip flow. Microscale Thermophys. Eng. 4, 303–320.

Arkailic, E.B., Breuer, K.S., Schimidt, M.A., 1994. Gaseous flow in microchannels. Application of microfabrication to fluid mechanics. ASME FED 197, 57–66.

Beskok, A., Karniadakis, G.E., 1994. Simulation of heat and momentum transfer in complex micro geometries. J. Ther. Heat Transfer 8, 647–653.

Bird, R.B., Armstrong, R.C., Hassager, O., 1987. Dynamic of polymeric liquids 1, second ed. John Wiley, New York.

Bird, R.B., Stewart, W.E., Lightfoot, E.N., 2002. Transport Phenomena. Wiley, New York.

Brochard, F., de Gennes, P.G., 1992. Shear-dependent slippage at a polymer/solid interface. Langmuir 8, 3033–3037.

Celeta, G.P., 2004. Heat Transfer and Fluid Flow in Microchannels. Begell House Publishers, Inc., New York.

Datta, A.K., 1999. Heat transfer coefficient in laminar flow of non-Newtonian fluid in tubes. J. Food Eng. 39, 285–287.

Eirich, F.R., 1978. Rheology: Theory and Applications, 3rd ed. Academic Press Inc. Ltd., New York.

Etemad, S.Gh., 1995. Non-Newtonian flow and heat transfer through non- circular channels. Ph.D., Thesis. Chemical Eng. Dept., McGill University, Montreal, Canada.

Golden, S., 1964. Elements of the Theory of Gases. Addison-Wesley, Reading, MA.

Harms, T.M., Kazmierczak, M.J., Gerner, F.M., 1999. Developing convective heat transfer in deep rectangular microchannels. Int. J. Heat Fluid Flow 20, 149–157.

Hill, D.A., 1998. Wall slip in polymer melts: a pseudo-chemical model. J. Rheol. 42, 581–601.

Koplik, J., Banavar, R., 1995. Continuum deductions from molecular hydrodynamics. Annual Rev. Fluid Mech. 28, 257–292.

Léger, L., Raphaël, E., Hervet, H., 1999. Surface-anchored polymer chains: their role in adhesion and friction. Adv. Polym. Sci. 138, 185–225.

Lin, Y.H., 1985. Explanation for slip-stick melt fracture in terms of molecular dynamics in polymer melts. J. Rheol. 29, 605–637.

Malkus, D.S., Nohel, J.A., Plohr, B.J., 1990. Dynamics of shear flow of a non-Newtonian fluid. J. Comp. Phys. 87, 464–487.

Maxwell, J.C., 1878. On the stresses in rarefied gases arising from inequalities of temperature. Phil. Trans. Roy. Soc. London 231, 249–255.

Mcleish, T.C.B., Ball, R.C., 1986. A molecular approach to the spurt effect in polymer melt flow. J. Polym. Sci. Polym. Phys. Ed. 24, 1735–1745.

Morini, G.L., 2004. Single-phase convective heat transfer in micro-channels: a review of experimental results. Int. J. Thermal Sci. 43, 631–651.

Mudawar, W., Qu, I., 2002. Analysis of three-dimensional heat transfer in micro-channel heat sinks. Int. J. Heat Mass Transfer 45, 3973–3985.

Owhaib, W., Palm, B., 2004. Experimental investigation of single-phase convective heat transfer in circular microchannels. Exper. Thermal Fluid Sci. 28, 105–110.

Paranjape, B.V., Robson, R.E., 1990. Comment on slip velocity at a fluid–solid boundary. Phys. Chem. Liq. 21, 147.

Patankar, S.V., 1980. Numerical Heat Transfer and Fluid Flow. Hemisphere publishing Co., New York.

Pit, R., Hervet, H., Leger, L., 2000. Direct experimental evidence of slip in hexadecane: solid interfaces. Phys. Rev. Lett. 85, 980–983.

Qu, W., Mala, M., Li, D., 2000. Heat transfer for water flow in trapezoidal silicon microchannels. Int. J. Heat Mass Transfer 43, 3925–3936.

Ruckenstein, E., Rajora, P., 1983. On the no-slip boundary condition of hydrodynamics. J. Colloid Interface Sci. 96, 488–491.

Shih, J.C., Ho, C., Liu, J., Tai, Y., 1996. Monatomic and polyatomic gas flow through uniform microchannels. In: National Heat Transfer Conf. Microelectromechanical Systems (MEMS), Atlanta, GA, pp. 197–203.

Simoes, E.W., Mansano, R.D., Furlan, R., Verdonk, P., 1998. Microfluidic amplifiers fabricated in silicon. In: Proceedings of the XIII SBMicro – International Conference on Microelectronics and Packaging ICMP'98, Curitiba, PR, Brazil, pp. 175–181.

Sparrow, E.M., Lin, S.H., 1962. Laminar heat transfer in tubes under slip-flow conditions. J. Heat Transfer 84, 363–369.

Tretheway, D., Meinhart, C., 2002. Apparent fluid slip at hydrophobic microchannel walls. Phys. Fluids 14, 9–12.

Tunc, G., Bayazitoglu, Y., 2000. Heat transfer for gaseous flow in microtubes with viscous heating. In: Proc. ASME Heat Transfer Div., HTD 366-2, pp. 299–306.

Tunc, G., Bayazitoglu, Y., 2001. Heat transfer in microtubes with viscous dissipation. Int. J. Heat Mass Transfer 44, 2395–2403.

Tunc, G., Bayazitoglu, Y., 2002. Heat transfer in rectangular microchannels. Int. J. Heat Mass Transfer 45, 765–773.

Wang, S-Q., 1999. Molecular transitions and dynamics at polymer/wall interfaces: origins of flow instabilities and wall slip. Adv. Polym. Sci. 138, 227–275.

Watanabe, K., Yanuar, Mizunuma, H., 1998. Slip of Newtonian fluids at slid boundary. JSME Int. J. Ser. B 41, 525–529.

Watanabe, K., Yanuar, Udagawa, H., 1999. Drag reduction of Newtonian fluid in a circular pipe with a highly water-repellant wall. J. Fluid Mech. 381, 225–238.

Yang, X., Wang, S.Q., Halasa, A., Ishida, H., 1998. Fast flow behavior of highly entangled monodisperse polymers. 1. Interfacial stick slip transition of polybytadiene melts. Rheol. Acta 37, 415–423.

Yogesh, M. Joshi, Ashish, K. Lele, Mashelkar, R.A., 2000. A unified wall slip model. J. Non-Newtonian Fluid Mech. 94, 135–149.

Zengerle, R., Richter, M., 1994. Simulation of microfluid systems. J. Micromech. Microeng. 4, 192–204.

Zhu, Y., Granick, S., 2001. Rate-dependent slip of Newtonian fluids at smooth surfaces. Phys. Rev. Lett. 87, 96.